A SMOKE STUDY OF THE MOTION OF

THE VORTICES SHED FROM THE TIPS OF

A TWO-BLADED MODEL HELICOPTER ROTOR

IN HOVERING FLIGHT

A THESIS

Presented to

the Faculty of the Graduate Division

by

Craig Eugene Swavely

In Partial Fulfillment

of the Requirements for the Degree

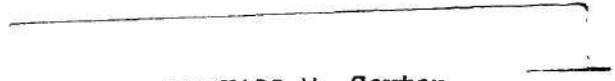Master of Science

Georgia Institute of Technology

December, 1958

A SMOKE STUDY OF THE MOTION OF

THE VORTICES SHED FROM THE TIPS OF

A TWO-BLADED MODEL HELICOPTER ROTOR

IN HOVERING FLIGHT

Approved:

Robin B. Gray

Walter Castles, Jr.

Charles W. Gorton

Date Approved by Chairman _December 15 1958_

ACKNOWLEDGMENTS

TABLE OF CONTENTS

LIST OF FIGURES

LIST OF SYMBOLS

a   slope of lift curve, per radian

A, C   geometric characteristics in wake equation, $\dfrac{r}{R} = A + Ce^{-\lambda\psi}$

c   blade chord, feet

C_T thrust coefficient, $C_T = \dfrac{T}{\rho\,\pi\,\Omega^2\,R^4}$

$C_\varkappa$ vortex strength coefficient, $C_\varkappa = \dfrac{\varkappa}{4\,\pi\,R^2\,A^2\,\Omega}$

K_1, K_2, K_3 coefficients in helix vertical displacement equations:

$$\frac{\Delta Z}{R} = K_1\,\Delta\psi \quad \text{for} \quad 0 = \psi < \pi$$

$$\frac{\Delta Z}{R} = K_2\,\Delta\psi \quad \text{for} \quad \pi < \psi < 3\pi$$

$$\frac{\Delta Z}{R} = K_3\,\Delta\psi \quad \text{for} \quad 3\pi < \psi = \infty$$

r   radius of point from axis of rotation, feet

R   rotor radius, feet

T   rotor thrust, pounds

Z   distance measured perpendicular to rotor plane, positive downward, feet

$\bar{x}$ nondimensional radius along blade, $\bar{x} = \dfrac{r}{R}$

θ blade element pitch angle, measured between zero lift chord and rotor plane, degrees

$\varkappa$ strength of tip vortex, square feet per second

λ exponent in wake equation, $\dfrac{r}{R} = A + C\,e^{-\lambda\psi}$

ρ mass density of air, slugs per cubic feet

P distance from point on blade to central curve of helical vortex, feet

ψ azimuth angle of rotor blade measured clockwise, radians

w axial induced velocity, feet per second

Ω angular velocity of rotor, radians per second

SUMMARY

The motion of the vortices shed from the tips of a hovering, two-bladed, model helicopter rotor was determined experimentally, and compared with the motion of the tip vortex of a single-bladed rotor. The experimental results were used to calculate a theoretical spanwise aerodynamic blade loading for a two-bladed rotor selected from NACA Technical Note 3688. A comparison was made of the calculated blade loading with an existing measured loading for that rotor.

The "teetering" type model rotor was four feet in diameter with a 2:1 blade taper ratio, and an NACA 43015 blade airfoil. Blade pitch angles of 5.4, 7.2, 9.0, and 9.9 degrees were tested in a speed range of 500 to 600 rpm. A rotor test mount was utilized to obtain rotor thrust, torque and rpm, and the data were recorded by an oscillograph. Moving pictures were taken of one of the tip vortices made visible by introducing smoke into the vortex core.

The smoke pictures revealed that the vortices shed from the tips of the two-bladed rotor initially had a greater nondimensional displacement toward the axis of rotation than the tip vortex shed from the single-bladed rotor, for the same blade azimuth positions and thrust coefficients. However, the wakes of both rotors reached the same ultimate wake contraction ratio. For the first half blade revolution, the tip vortices of the two-bladed rotor had a smaller nondimensional vertical displacement than the tip vortex of the single-bladed rotor for identical thrust coefficients. The nondimensional vertical displacement of

the tip vortices for the two-bladed rotor increased with the approach of
the second blade, and after one blade revolution was larger than the non-
dimensional displacement of the tip vortex for the single-bladed rotor.
The calculated induced-velocity distribution, based on the model data,
yielded a theoretical spanwise aerodynamic blade loading for the NACA
two-bladed rotor which was in excellent agreement with existing measured
values.

It appears from the results of this study that a set of induced-
velocity distribution charts, based on the pattern of the model tip vor-
tices, should be computed for a practical range of thrust and tip vortex
strength coefficients. Such a set of charts would permit calculation of
a theoretical spanwise blade loading for any practical two-bladed rotor,
regardless of blade planform. It should be emphasized here that the cal-
culation of the charts would be quite lengthy. In any future experiments
of this nature, consideration should be given to setting the calculations
up on a computer to save time and gain accuracy.

CHAPTER I

INTRODUCTION

The smoke visualization method of analyzing air flow patterns lends itself well to a study of the geometrical characteristics of wakes. A work by Gray (1)[x], utilizing motion picture photography of smoke introduction into the air flow, made an analytical and experimental investigation of the helical vortex shed from the tip of a single-bladed model helicopter rotor. The results of this work led the present investigator to apply the methods and theory developed therein to a two-bladed rotor, and to compare the tip vortex pattern for the two rotors.

The air flow visualization studies lead to a calculation of a non-dimensional induced-velocity distribution along the blade based on the strength of the tip vortex. These induced velocities may then be applied to any other two-bladed rotor with the same tip vortex strength coefficient to obtain a theoretical spanwise blade loading. This analysis indicates better agreement with measured loadings than most present day methods.

Scott (2) supplemented this work with an experimental determination of the motion of a vortex sheet in the wake of a hovering rotor using a smoke visualization method.

---

[x]Numbers in parentheses refer to items in the bibliography.

CHAPTER II

INSTRUMENTATION AND EQUIPMENT

Model rotor blades.--The smoke studies were conducted in a closed room
43 feet long, 16 feet wide, and 12 feet high. A two-bladed, "teetering"
type rotor with no coning or lag angle was mounted in the center of the
room out of ground effect. The airfoil section of the blade began at a
distance of 4.5 inches from the axis of rotation. The blades were con-
structed with a steel leading edge, laminated walnut trailing edge, a
square tip, and had the following characteristics:

Diameter .... 4 feet

Blade section (no twist) ....NACA 43015

Blade chord

root chord (extended) .... 3.016 inches

tip chord .... 1.508 inches

Taper ratio 2:1

The blade collective pitch could be manually varied over a range of
angles from zero to ten degrees.

Rotor test mount.--The rotor was mounted on the aluminum rotor shaft of
the rotor test mount shown in Figure 1. Concentric with the rotor shaft
was an outer aluminum tube fixed to a supporting framework, and an inner
aluminum tube free to rotate as shown in Figure 2. A timing belt drive
turned the hub pulley on the inner aluminum tube, which turned the rotor
shaft through a ball bearing and slip universal joint assembly. A beam

strain-gage supported the weight of the rotor and rotor shaft, and an aluminum diaphragm acted as a centering device. The aluminum diaphragm offered little resistance to the vertical movement of the rotor shaft as compared to the resistance of the strain-gage arm. A pitch adjustment yoke mounted on the rotor shaft permitted blade pitch angle change, and also acted as a flapping stop. The smoke agent, titanium tetrachloride, was contained in a reservoir mounted on top of the hub pulley. A "T" connection joined a metal tube through the center of each blade to a neoprene tube running through the center of the rotor shaft to the reservoir. Centrifugal force pumped the smoke agent through the blades and, upon contact with the air at the blade tips, a dense white smoke was produced. A one-half horsepower, 24-volt, direct current, aircraft motor supported by ball bearings on its output shaft was used to drive the rotor as shown in Figure 3. As power was transmitted to the timing belt drive, the motor housing was prevented from rotating by a beam strain-gage which measured the torque. The strain-gage arm made contact with the motor housing through the outer race of a ball bearing mounted at the end of the arm to insure only simple bending in the arm. A 24-volt, direct current generator was driven through a timing belt by a one-horsepower, three-phase, induction motor operating from a 220-volt commercial power source to power the aircraft motor as shown in Figure 4. A rectifier energized the field of the driving motor, and supplied voltage, regulated by a 98-ohm rheostat acting as a voltage divider, to the field of the generator, which in turn supplied the armature of the aircraft motor. This allowed the rotor to be varied in speed from zero to approximately 600 rpm. The output and field voltage, and current of the generator, and the field

voltage of the driving motor were monitored by combination ammeter-volt-meters. A commutator was mounted on the hub pulley, and a set of brushes made contact once every revolution of the rotor blade. A flashlight battery supplied a signal to the oscillograph when the circuit was closed. Thrust and torque signals from the strain-gage beams were fed through an amplifier and recorded by an oscillograph shown in Figures 5 and 6. To indicate the azimuth position, ψ , of the rotor blade, a selsyn generator was driven through a two to one gear reduction ratio by the timing belt, and in turn drove a selsyn motor with a dial face and indicator which was photographed by the movie camera.

Camera and lighting.--A bank of six 300-watt reflector flood lights, placed directly under the rotor and perpendicular to the axis of a 16 mm Bell and Howell movie camera, provided a plane of light in an otherwise darkened room. The movie camera, mounted eight feet from the rotor, photographed a section view of the flow field normal to the camera axis. The camera was equipped with a 16 mm, f 1.6 lens and operated at 64 frames per second.

CHAPTER III

PROCEDURE

Calibration.--A static calibration was performed on the strain-gage arms prior to the actual test. Weights in half pound increments up to three pounds were suspended on the rotor shaft with the rotor removed, and an oscillograph record made as the thrust strain-gage arm was loaded and then unloaded. An average value of the displacement of the oscillograph trace was used to convert thrust strain-gage deflection to thrust. The torque strain-gage arm was removed from the test mount, and increments of half pound weights up to five pounds were hung directly on the arm for a calibration. The test mount was run with the rotor removed, and known weights hung from the rotor shaft to obtain a friction torque calibration. This was not performed with the same amplifier and recorder as used in the actual tests. To obtain a zero reference for the blade collective pitch angles, the yoke pitch change linkage was adjusted until the oscillograph and smoke filaments indicated that the rotor was producing no thrust. The linkage was calibrated so that it could be manually changed to give the desired blade angle.

Test procedure.--The following procedure was used for the four blade-collective pitch angles tested: The amplifier was turned on about one hour prior to actual running to allow it to warm up. The oscillograph was turned on about five minutes before running for warm up. Next, the rectifier was turned on, and the motor-generator unit started. The amplifier

was adjusted to balance out the circuits, and the combination ammeter-voltmeters checked for the proper current and voltage. The titanium tetrachloride was loaded into the reservoir, and the blade tip checked for good smoke. The camera lights were then turned on, and a short identifying moving picture taken with the 16 mm movie camera. The room temperature and barometric pressure were recorded. A zero reading of the torque strain-gage arm was obtained by activating the oscillograph. Because the lower bearing was not mounted squarely on the inner shaft, the oscillograph recorded a large oscillation in the thrust reading at low rotor angular velocities. Therefore, with the rotor stopped an average thrust reading would not be recorded. To get a zero thrust-gage reading, the rotor was run very slowly so that no measurable thrust was produced, but an average value of the recorded oscillation could be obtained. At higher rotor angular velocities the oscillation was damped out by a low pass filter in the recorder circuit. The rotor was next brought up to 500 to 600 rpm and allowed to run until a steady state condition was reached. The movie camera and oscillograph were simultaneously activated for two to three seconds. The rotor was then slowed down until it produced no measurable thrust and the oscillograph activated for a second zero thrust reading. The rotor was stopped and again the oscillograph recorded a zero torque reading.

Reduction of data.--A zero torque strain-gage reading was obtained by averaging the oscillograph zero reading with the rotor stopped at the beginning and, at the end of each run. The torque oscillograph trace displacement was corrected for the zero reading and friction torque, and converted to the force on the strain-gage arm by use of the calibration

curve. This value was multiplied by the length of the torque strain-gage arm and the ratio of motor and hub pulleys to give the shaft torque. Using this torque, a torque coefficient was calculated for each blade angle tested. It was found that the thrust strain-gage trace drifted when the recorder was turned on, and slowly returned with the recorder off. The zero reading at the end of the run was selected as being the most accurate since the elapsed time between the run and the final zero reading was small. The thrust strain-gage displacement trace was corrected with this zero reading, and converted to thrust from the calibration curve. The rotor thrust coefficient, $C_T = \dfrac{T}{\rho \pi \Omega^2 R^4}$, was calculated, and checked by calculating a theoretical C_T by the method of (3). A lift curve slope of 7.0, as obtained from (4), was used in the theoretical calculation because of the low Reynolds number at which the tests were run. A comparison of the experimental and theoretical values of C_T revealed the experimental value to be one half of the value obtained from the theoretical calculation. The calculated values were checked by two other theoretical methods, and all were found to agree. It was concluded that the error in the experimental values was in the instrumentation, but it was not possible to check this because this particular instrumentation had since been replaced. Since the new instrumentation gave C_T values identical with those calculated from the theory of (3), the theoretical values were used in all later calculations.

Because the vortex from either blade traced the same path, only the tip vortex from one blade was considered. A frame by frame analysis of the motion pictures gave the radial and vertical displacement of the tip vortex as a function of blade azimuth position. The motion of a tip

vortex element was traced by plotting its location for a particular blade azimuth angle from a one-quarter scale projection of the film. A sequence of photographs showing the movement of the tip vortex is shown in Figure 7. From this data, nondimensional vertical and radial displacement versus blade azimuth position plots were made as described in (1). An equation of the form

$$\bar{x} = A + C e^{-\lambda \psi}$$

where:

ψ = blade azimuth position

r = local radius

R = radius of rotor

$\bar{x}$ = nondimensional radius along the blade, $\dfrac{r}{R}$

A, C, λ = geometric constants

was fitted to the radial displacement curve, and a comparison made of the geometrical characteristics of the tip vortex for a two and a one-bladed rotor in terms of the constants A, C, and λ. The value of A, as shown in Figure 8, is constant at 0.725. Momentum considerations gave a theoretical value for A equal to 0.707. The vertical displacement curve approximated a straight line with a change in slope at a blade azimuth angle of π and 3π radians. A comparison between the slopes, K_1, K_2, K_3, of the vertical displacement curves for a two-bladed rotor, and for the single-bladed rotor of (1), is shown in Figure 9.

The equation for the axial induced-velocity along the blade axis, as given in (1), was modified to correspond to the tip vortex pattern of a two-bladed rotor. The axial induced-velocity, w , for the tip

vortex of one of the blades is given by

$$\omega = \frac{\varkappa}{4\pi R A}\left\{\int_0^\pi V_{Z_o}\frac{d\psi}{P_{o_1}^3} + \int_\pi^{3\pi} V_{Z_o}\frac{d\psi}{P_{o_2}^3} + \int_{3\pi}^\infty V_{Z_o}\frac{d\psi}{P_{o_3}^3}\right\}$$

where:

$$V_{Z_o} = -\frac{\bar{x}}{A}\left\{\left[1+\frac{c}{A}e^{-\lambda\psi}\right]\cos\psi + \left[\frac{c}{A}\lambda e^{-\lambda\psi}\right]\sin\psi\right\} + \left[1+\frac{c}{A}e^{-\lambda\psi}\right]^2$$

$$\left\{\begin{matrix}P_{o_1}^2\\P_{o_2}^2\\P_{o_3}^2\end{matrix}\right\} = \left(\frac{\bar{x}}{A}\right)^2 - 2\left(\frac{\bar{x}}{A}\right)\left[1+\frac{c}{A}e^{-\lambda\psi}\right]\cos\psi + \left[1+\frac{c}{A}e^{-\lambda\psi}\right]^2$$

$$+ \left\{\begin{matrix}\left(\frac{K_1}{A}\right)^2\psi^2\\[6pt]\left(\frac{K_1}{A}\right)^2\left[\pi\left(\frac{K_1}{K_2}-1\right)+\psi\right]^2\\[6pt]\left[\left(\frac{K_2}{A}\right)\left[\frac{K_1}{K_2}\pi+2\pi\right]+\frac{K_3}{A}(\psi-3\pi)\right]^2\end{matrix}\right\} + \left(\frac{\varepsilon}{R A}\right)^2$$

P = distance from point on blade to central helical vortex

$\mathcal{X}$ = strength of tip vortex

ϵ = radius of core of helix

To indicate the use of this equation, a thrust coefficient equal to 0.00518 and a corresponding blade angle of 9.4 degrees was selected as an example. The $\bar{x}$ values of $\pm$ 0.2, $\pm$ 0.4, $\pm$ 0.6, $\pm$ 0.8, $\pm$ 0.9, $\pm$ 0.975, $\pm$ 1.0 were chosen to define the induced-velocity distribution across the blade. The resulting calculated velocities were added at corresponding stations to give the nondimensional induced-velocity distribution due to both tip vortices. The distribution across both blades was assumed to be identical, and the calculated induced-velocity distribution across one blade due to the tip vortices is shown in Figure 10. To find the total induced-velocity distribution, the effect of the sheet had to be taken into account. From the equation

$$ \mathcal{X} = \frac{1}{2}\ c\ \mathcal{R}\ R\ \bar{x}\ a\ \left(\theta - \frac{w}{\mathcal{R}\ R\ x} \right) $$

where:

c = blade chord

$\mathcal{R}$ = rotor angular velocity

a = slope of lift curve

θ = blade pitch angle

as given in (1), values of the blade bound vortex strength were found at the previous $\bar{x}$ stations using the induced-velocity distribution for the tip vortices only. The peak value was taken to be the strength of the

tip vortex. Here the assumption was made that any vortices shed along the blade would have an effect inboard of that particular station only. A new induced-velocity distribution was then calculated by the method of (5) using the blade bound vortex distribution as calculated above. Another bound vortex distribution was calculated using the new induced-velocity distribution, and the reiteration process repeated until no appreciable changes occurred in the induced-velocities. The final nondimensional axial induced-velocity distribution is shown in Figure 10. The aerodynamic spanwise blade loading was calculated using the final induced-velocity distribution in the blade element theory

$$\frac{d\,t}{d\,r} = \frac{1}{2}\,\rho\,c\,\Omega^2\,R^2\,\bar{x}^2\,a\left(\theta - \frac{w}{\Omega\,R\,\bar{x}}\right)$$

where: ρ = mass density of air

The blade loading curve was plotted, and when integrated, a thrust of 1.03 pounds was obtained in comparison with the experimental value of 1.09 pounds as shown in Figure 11.

The nondimensional induced-velocity distribution, due to the tip vortex only, may be applied to any other two-bladed rotor with the same tip vortex strength coefficient, $C_\varkappa = \dfrac{\varkappa}{4\,\pi\,R^2\,A^2\,\Omega}$, to obtain a theoretical spanwise blade loading. To check this, the above procedure was followed for the conditions given in Figure 9, page 22 of (6). The calculated blade loading resulted in much higher values than the measured loading using the blade pitch angle of 9.2 degrees as given in (6). A tip vortex strength coefficient, calculated using the peak blade loading

of (6), was found to agree with the model tip vortex strength coefficient. Therefore, the nondimensional induced-velocity distribution due to the tip vortex should be the same for the model and for the rotor of (6). When the blade pitch angle of 9.2 degrees, given in (6), was used to calculate a vortex strength coefficient, larger values were obtained than those for the model. This seemed to indicate a lower blade angle than that given in (6) should be used. For a blade pitch angle of 6.68 degrees, the calculated and measured loading curves were in agreement as shown in Figure 12.

CHAPTER IV

DISCUSSION OF RESULTS

The thrust coefficients obtained from experimental data with the
original instrumentation did not agree with the calculated theoretical
thrust coefficients. However, when like tests were run with different
instrumentation, the experimental values of C_T agreed with the theoreti-
cal values. Therefore, it was concluded that the original instrumenta-
tion was in error, and the calculated values of the thrust coefficients
were assumed to be valid.

A comparison between the geometrical quantities in the wake con-
traction equation for a two-bladed and a single-bladed rotor at a given
blade azimuth position and thrust coefficient, revealed a greater nondi-
mensional axial displacement of the wake for the two-bladed rotor as
shown in Figure 8. This meant the paths of the tip vortices in the wake
of the two-bladed rotor were moving nondimensionally further inboard than
the tip vortex path of a single-bladed rotor, as might be expected with
the addition of another blade. However, both wakes approached the same
ultimate wake contraction ratio. The vertical displacement curve was
divided into three straight lines with a change in slope at π and 3π
radians. The increase in slope was due to the effect of the far blade
(far blade in reference to the increment of vortex photographed) passing
over the section of tip vortex being considered. Smaller breaks were ob-
served at 2π radians, 4π radians, and so on, but were within the scatter

of the data, and were not taken into account. The vertical displacement coefficients, shown in Figure 9, indicate that for the first half blade revolution the tip vortices of the two-bladed rotor had a smaller nondimensional vertical displacement than the tip vortex of the single-bladed rotor for the same C_T. This was attributed to the greater nondimensional radial motion of the vortices in the case of the two-bladed rotor. However, after a blade revolution, the tip vortices for the two-bladed rotor had a larger nondimensional vertical displacement because of the influence of the second tip vortex.

The theory of (1), modified to apply to a two-bladed rotor, yielded a spanwise blade loading distribution which integrated to give a thrust of 1.03 pounds as compared with 1.09 pounds from experimental data as shown in Figure 11. It must be noted here that the method of (5), used to calculate the velocity at the sheet, was only approximate. Other more accurate theoretical methods might be used (i.e. considering the individual helical vortex filaments in the sheet) but it was felt that the amount of work involved was prohibitive for the accuracy gained. Also, the induced velocity distribution due to the tip vortex, as shown in Figure 10, is not exact. Because of the nature of the integral in the modified equation of (1) for the axial induced-velocity, a graphical integration was performed, and a larger number of points to define the curve would have yielded a more accurate result. On account of the length of the calculations involved, only a minimum number of points to plot the curve were taken After a blade azimuth angle of 6 π radians, the contribution of induced velocity was so small that extrapolated values were used.

It must be remembered that the same approximation made in calculating the induced velocities for the model rotor also hold for the calculation of induced velocities for comparison with (6). The comparison of the calculated spanwise blade loading using these induced velocities with the measured blade loading of (6), and the loading calculated by several other theoretical methods, is shown in Figure 12. This calculated loading would not check the measured blade loading when the blade of 9.2 degrees, as given in (6), was used. However, (6) states that an unexplainable decrease in chordwise blade loading at the tip (other than due to tip loss) was obtained. The blade was checked for a reflex at the trailing edge or blade twist, but no deformities were measured. The report continues to say that the effect may have been because of an increase in the boundary layer toward the tip from rotation effects, which could give the blade an effective negative camber. This effect would tend to decrease the blade pitch angle. When an angle of 6.68 degrees was used, the theoretical and measured blade loadings correspond as shown in Figure 12. Also, as noted in the data reduction, when a tip vortex strength coefficient was calculated using the peak blade loading of (6), it agreed with the model tip vortex strength coefficient. This means the nondimensional induced-velocity distribution resulting from the tip vortices should be the same for the model and for the rotor of (6). However, when the blade pitch angle of 9.2 degrees given in (6) was used to calculate a vortex strength coefficient, larger values were obtained than those for the model. This seemed to indicate a lower blade angle than that given in (6) should be used. An effect not mentioned in (6) was that of dynamic twist. If the blade trailing edge was to reflex only slightly,

a comparatively large change in the blade zero lift line would result. Also, at test rpm there could be a deflection in the pitch change linkage tending to reduce the blade pitch angle. All of these effects would tend to add to give a lower blade pitch angle. It also might be noted here that the slight difference in the theoretical and measured loadings of Figure 11 could be resolved if the NACA blade had an effective linear washout.

CHAPTER V

CONCLUSIONS

An experimental study of the motion of the vortices shed from the tips of a two-bladed rotor in hovering flight indicates that:

1. The vortices shed from the tips of a two-bladed rotor have a greater nondimensional displacement toward the axis of rotation than the tip vortex shed from a single-bladed rotor, for the same blade azimuth positions and thrust coefficients.

2. The tip vortex reaches the same ultimate wake contraction ratio for a two-bladed and a single-bladed rotor.

3. For the first half blade revolution, the nondimensional vertical displacement of the tip vortices for a two-bladed rotor is less than that of a single-bladed rotor, for the same thrust coefficients.

4. After one blade revolution, the nondimensional vertical displacement of the tip vortices for a two-bladed rotor is greater than the vertical displacement of the vortex of the single-bladed rotor, for identical thrust coefficients.

5. The calculated nondimensional induced-velocity distribution, associated with the tip vortices of the model, may be used to calculate a theoretical spanwise aerodynamic blade loading for any two-bladed rotor with the same tip-vortex strength coefficient as for the model.

6. It appears that the results of this study warrant a further computation of induced-velocity distributions, based on the tip vortex

pattern of a two-bladed rotor for a practical range of thrust and vortex strength coefficients, to permit calculation of a theoretical spanwise aerodynamic blade loading for any practical two-bladed rotor, regardless of blade planform.

CHAPTER VI

RECOMMENDATIONS

An accurate determination of the spanwise aerodynamic blade load-
ing is essential in rotor stress analysis. It would therefore be de-
sirable to apply the model tip-vortex induced-velocity distribution to a
calculation of blade loadings for a practical range of thrust and tip
vortex strength coefficients for a two-bladed rotor. To extend the use-
fulness of the method further, ranges of tip vortex strength coefficients
for a range of forward flight velocities could be computed. It should be
emphasized here that the calculations are quite lengthy and, to save time
and gain accuracy, should be set up on a computer.

An interesting extension of the first part of this thesis would
be to compare the wakes of rotors of more than two blades with the exist-
ing data.

APPENDIX
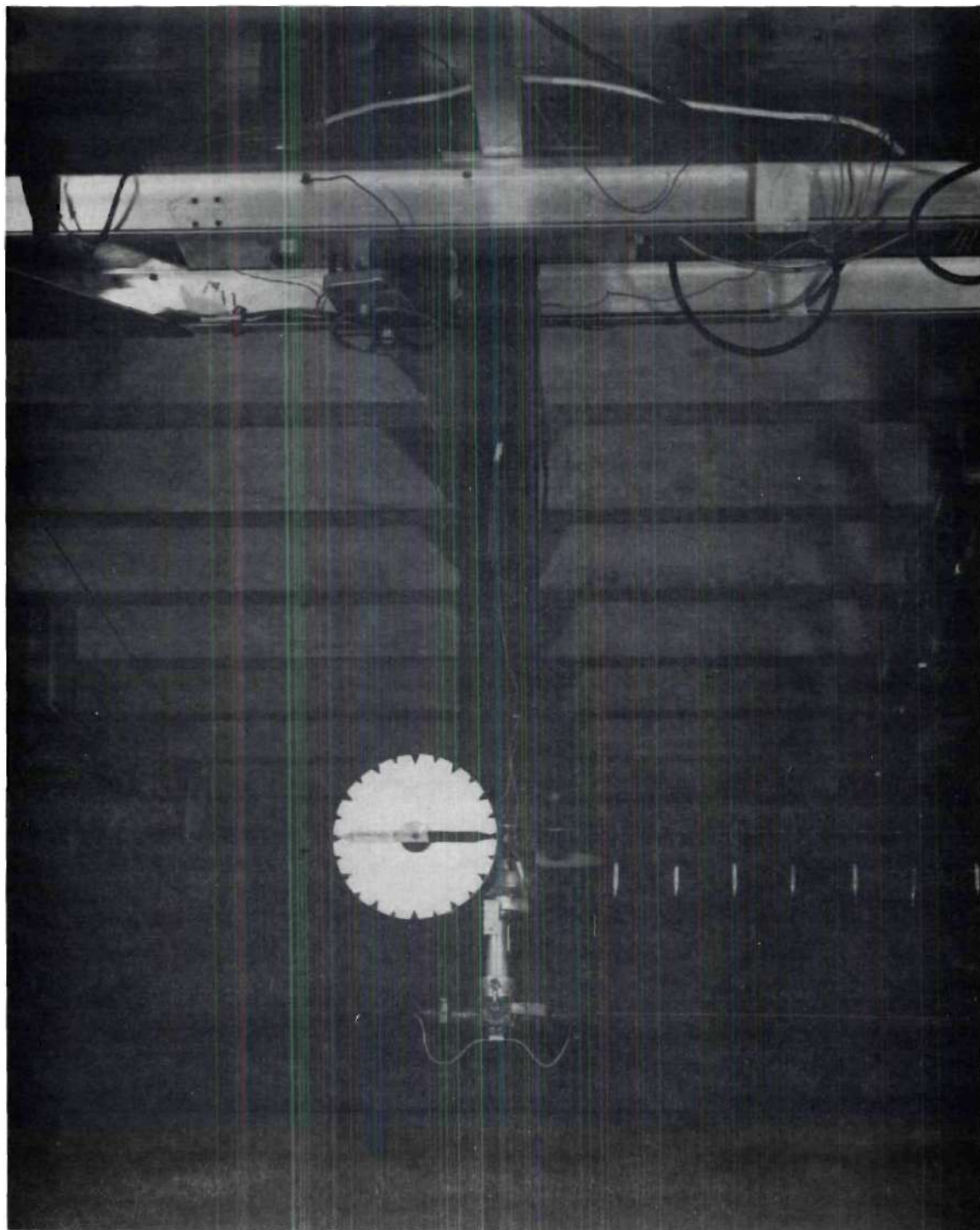
Figure 1 Rotor Test Mount and Rotor Blade
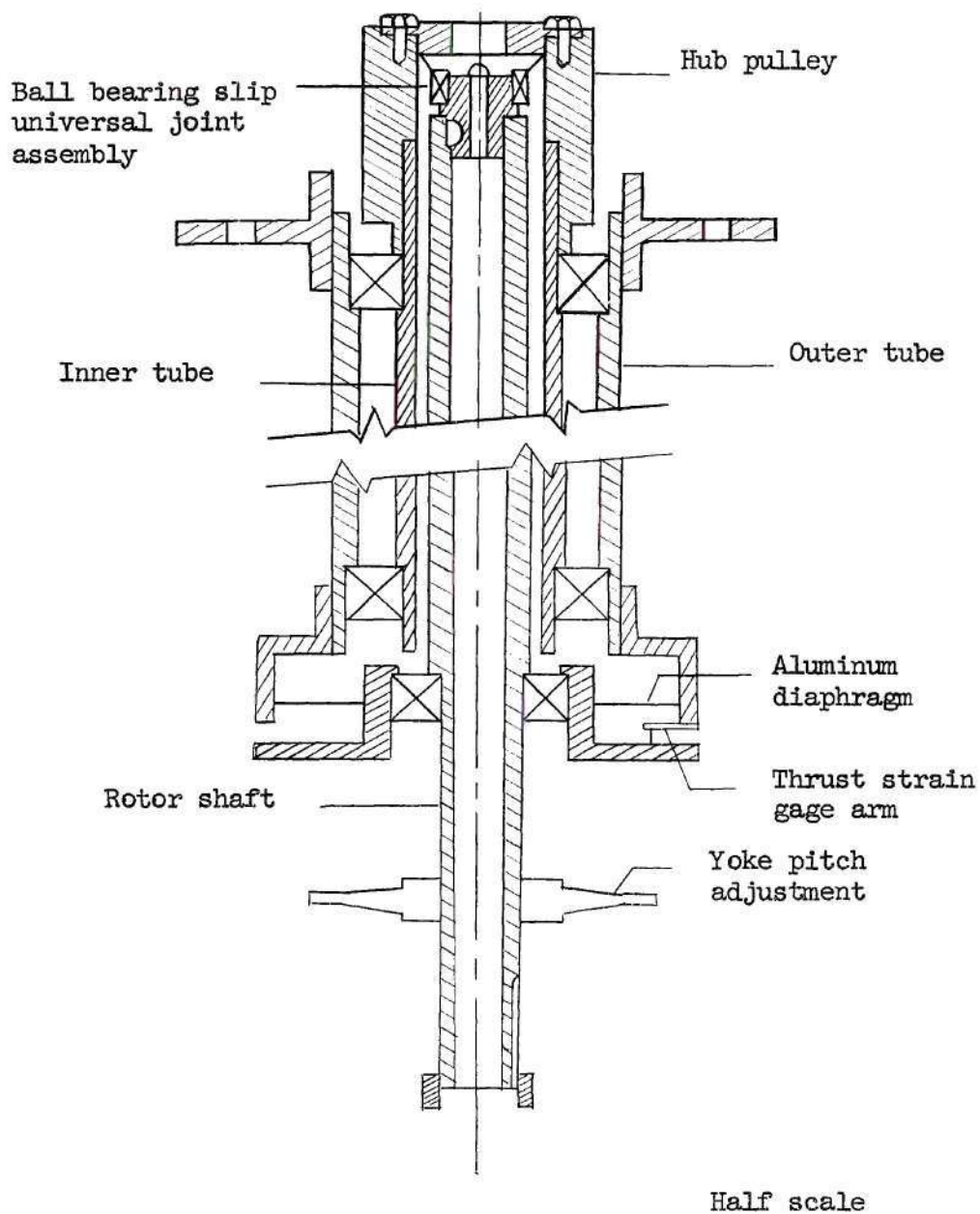
Figure 2 Cross-Section Drawing of Rotor Test Mount
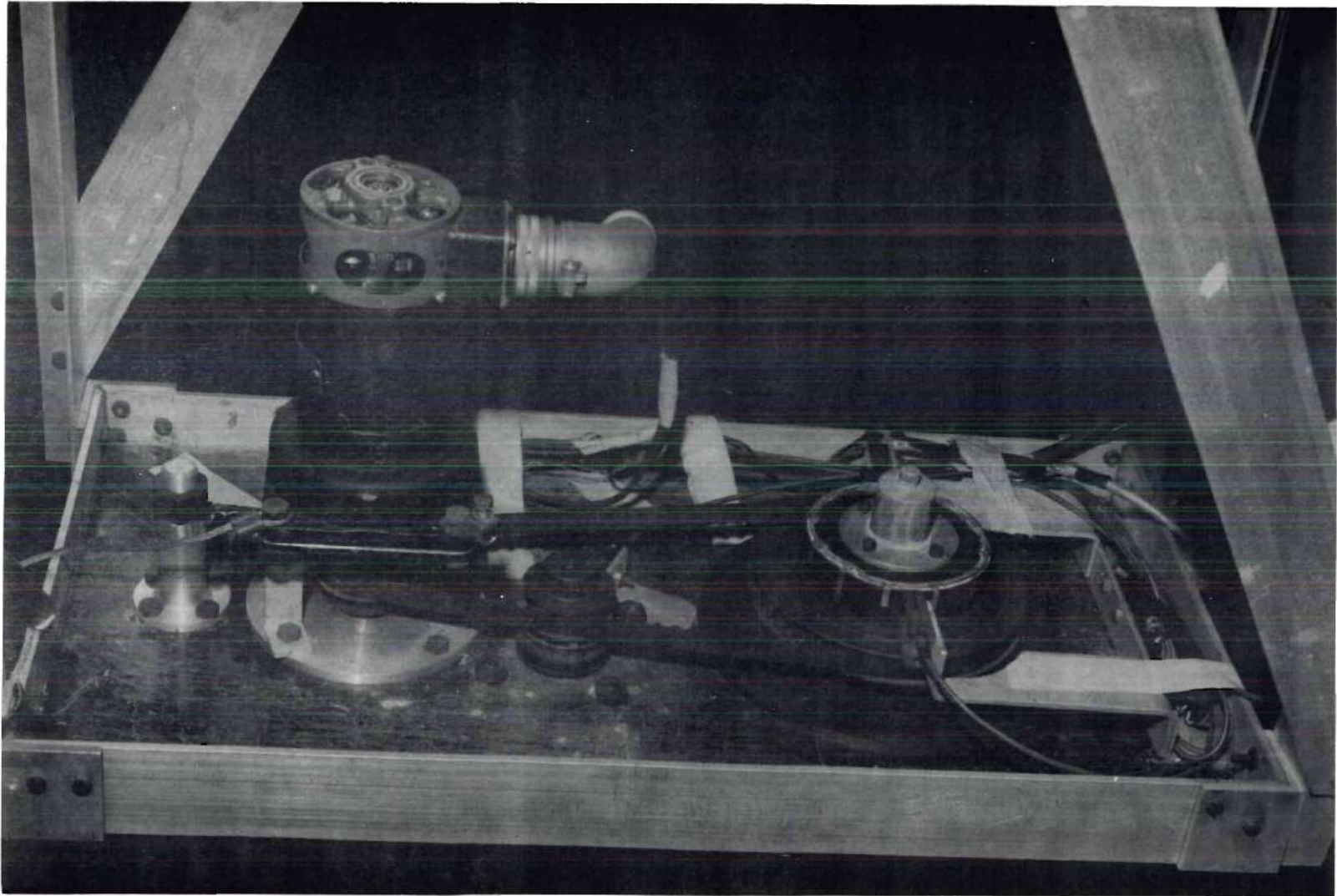
Figure 3   Rotor Test Mount Showing Driving Motor
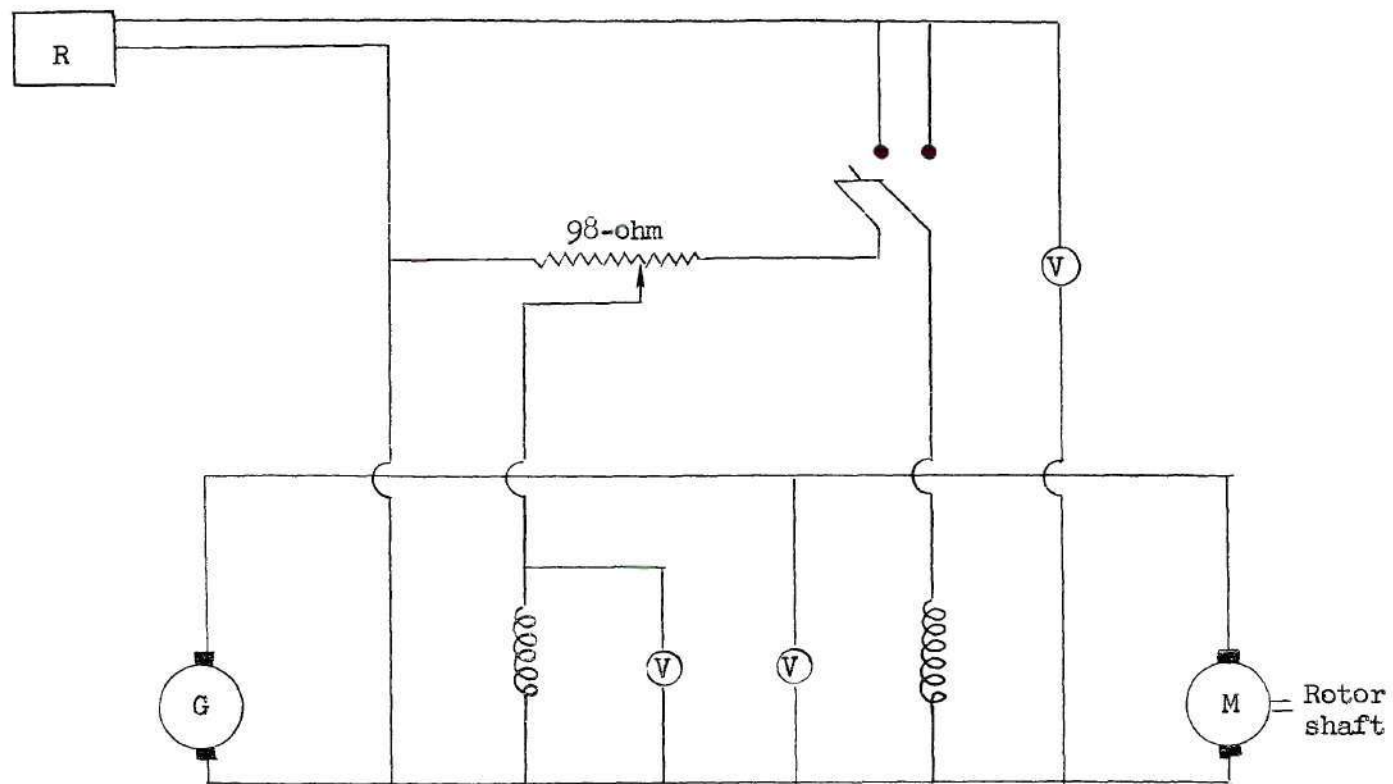
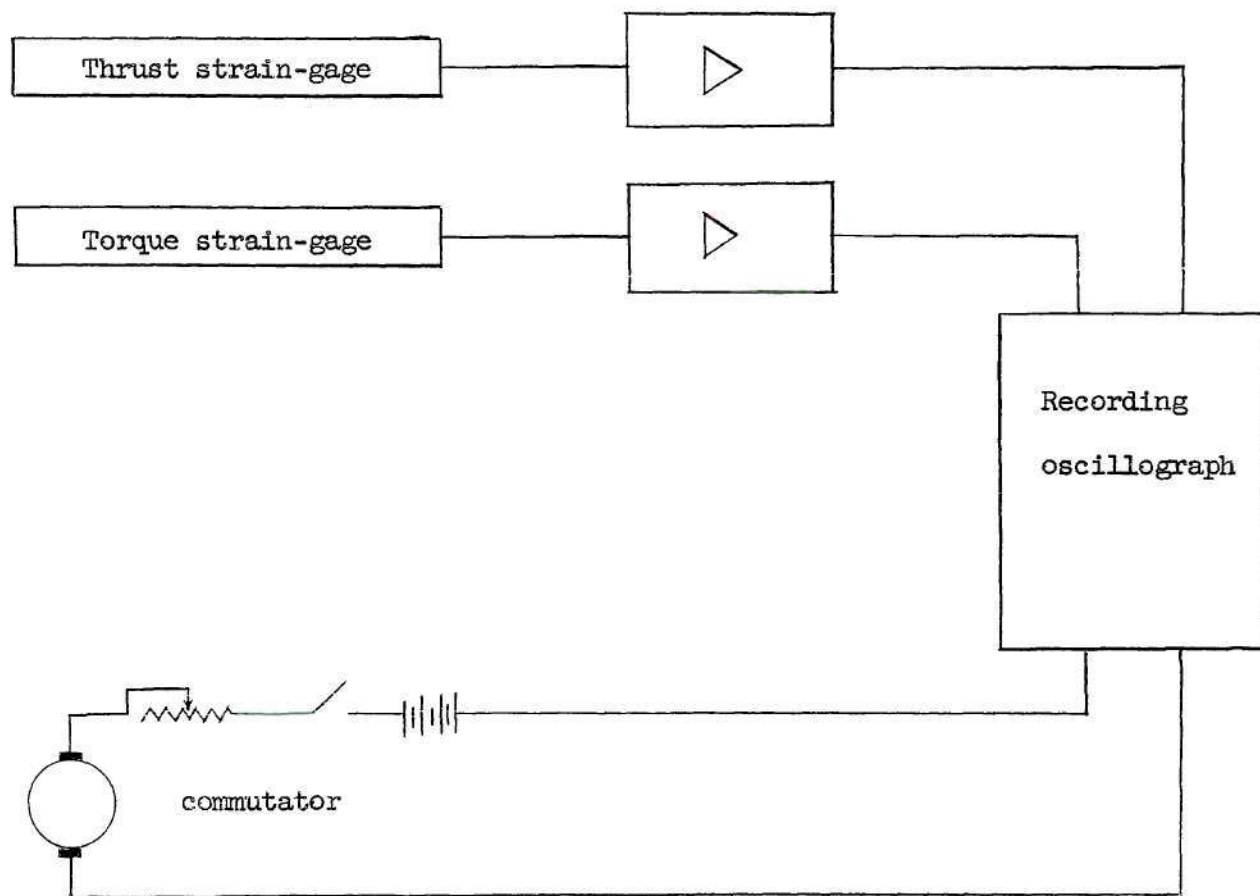Figure 4   Rotor Test Mount Circuit Diagram

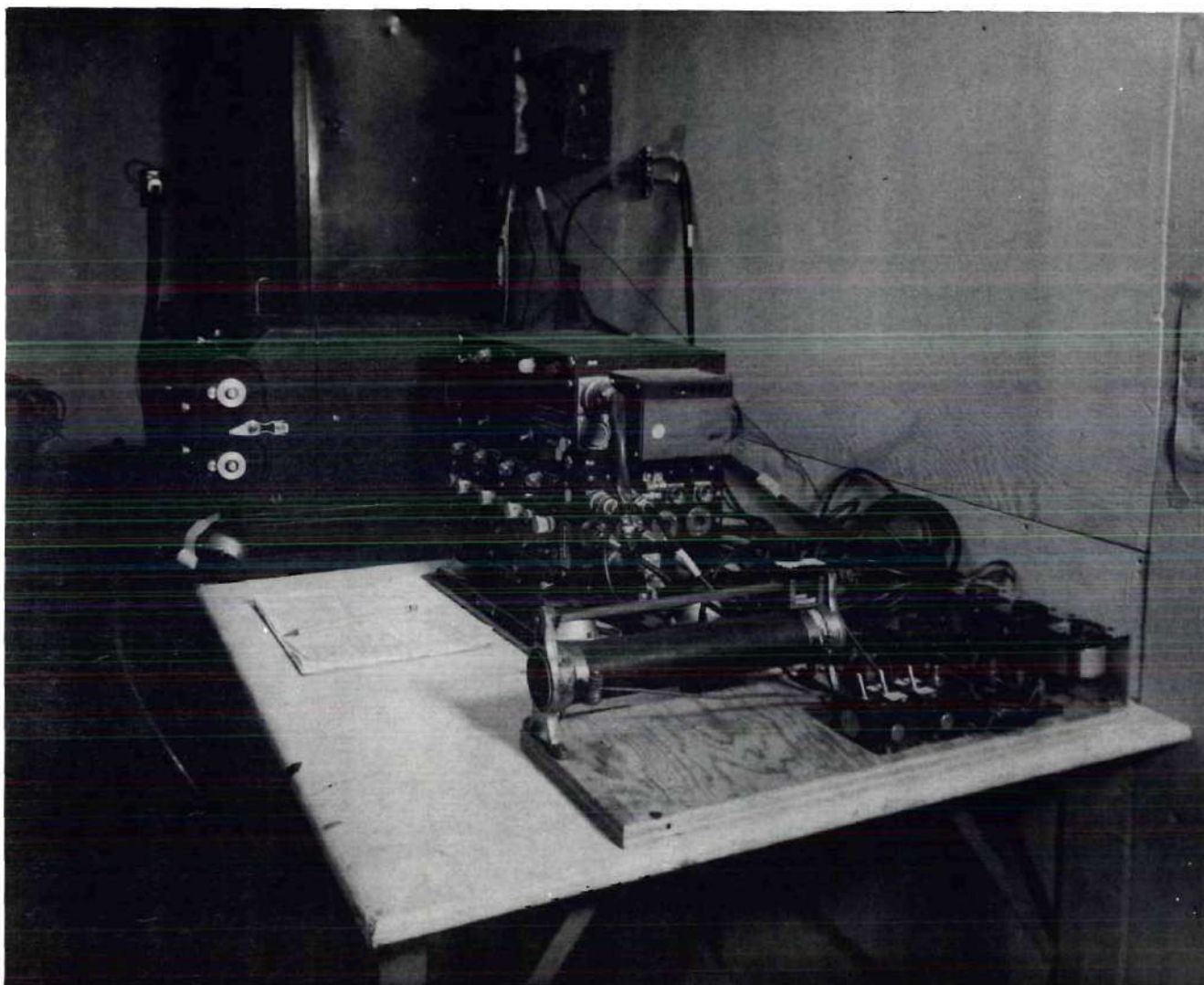Figure 5   Instrumentation Circuit Diagram

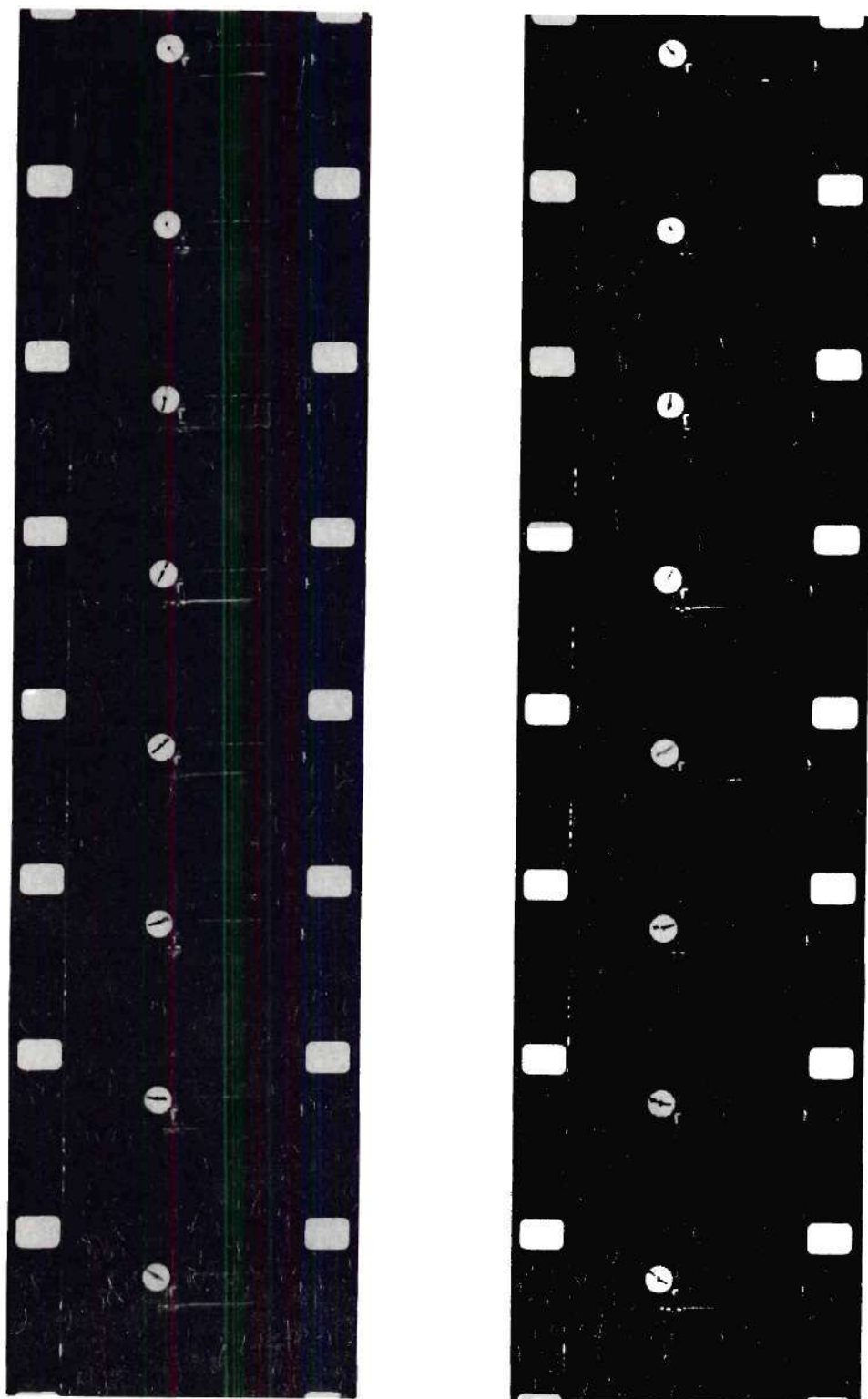Figure 6 Amplifier, Power Supply and Recording Oscillograph

Figure 7 Photographs of the Tip Vortex in the Wake
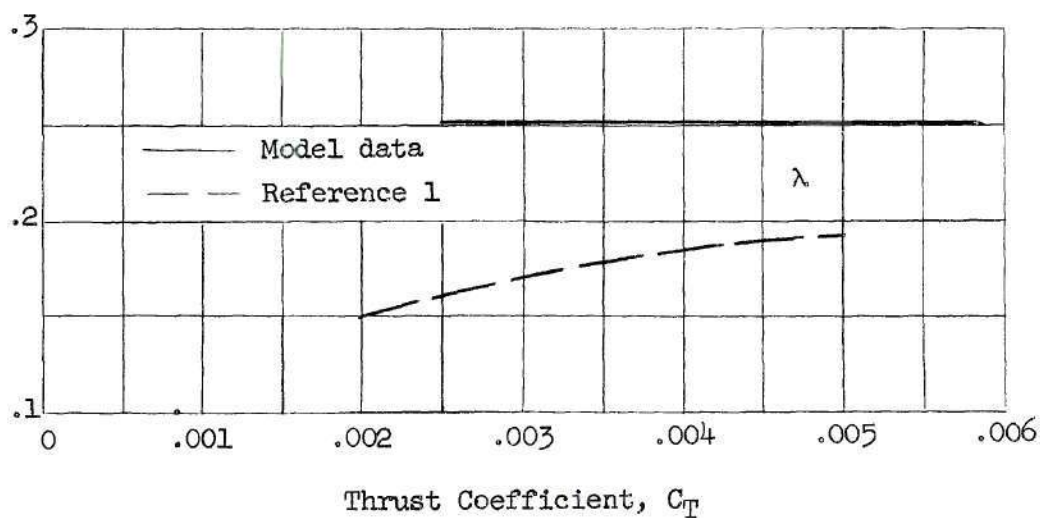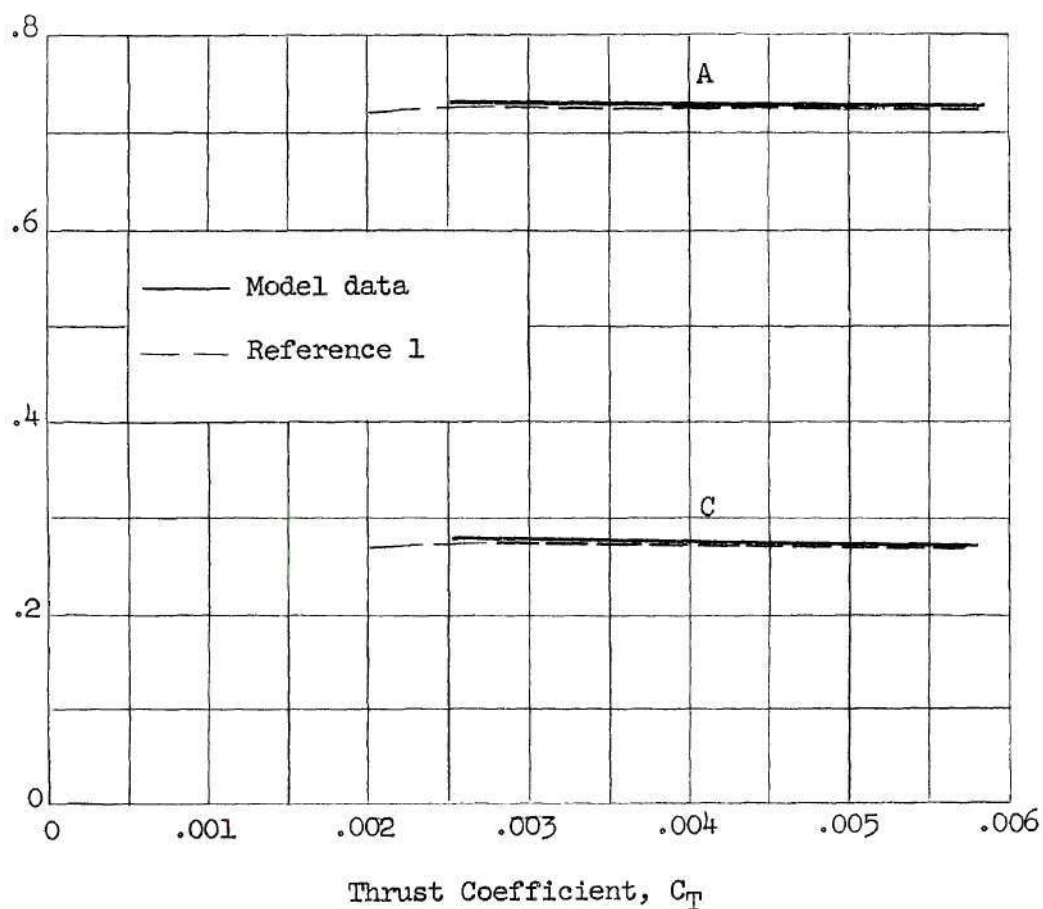
of a Two-Bladed, Hovering Rotor

Figure 8 Variations of Geometric Quantities in the Wake Contraction Equation, $\frac{r}{R} = A + C e^{-\lambda \psi}$, with Thrust Coefficient for a Two-Bladed Rotor, and a Comparison with those for a Single-Bladed Rotor.
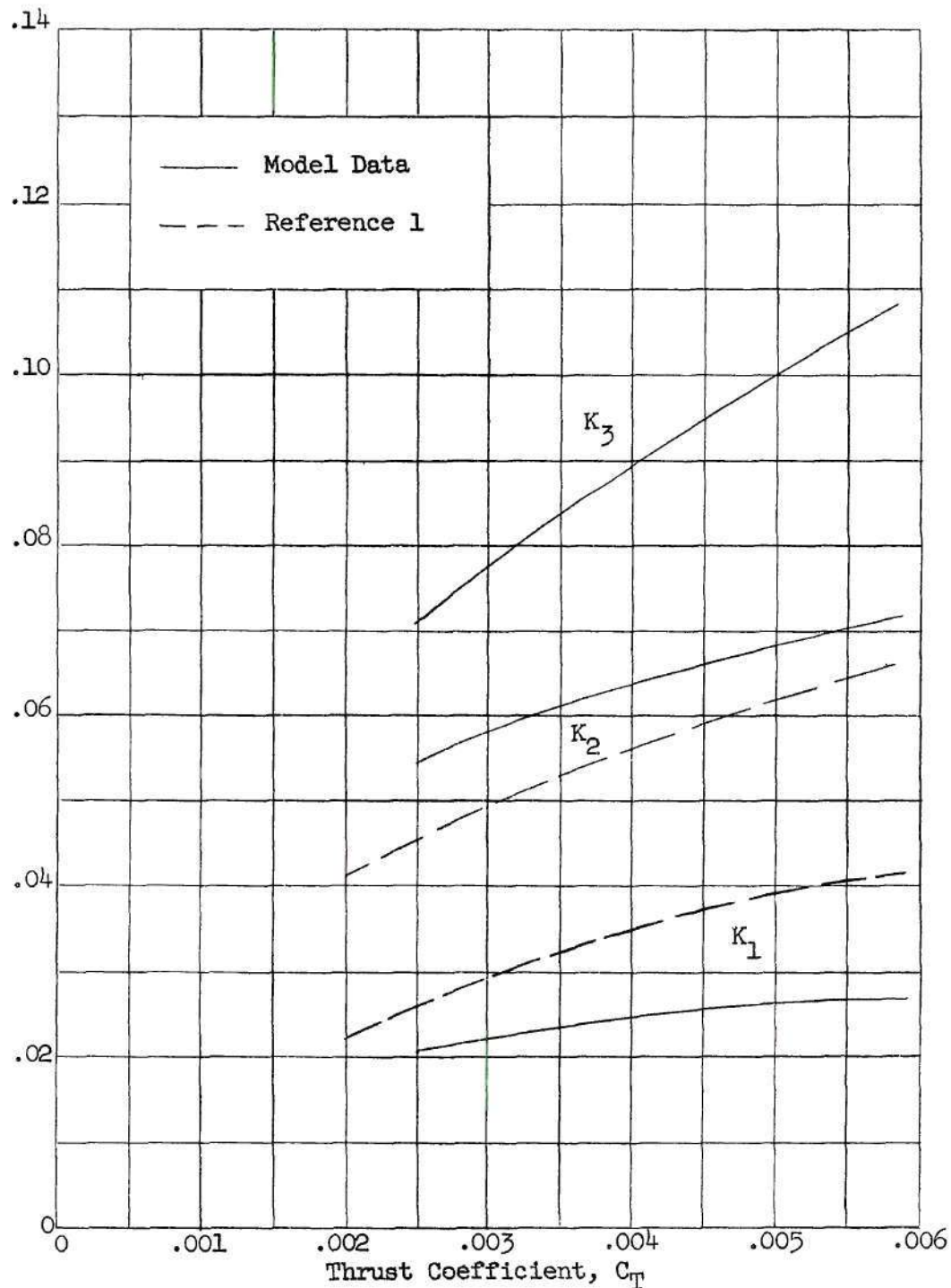
Figure 9 Variation of Coefficients in Vertical Displacement Equation $\frac{\Delta Z}{R} = K_1 \Delta \psi$ for $\psi < \pi$, $\frac{\Delta Z}{R} = K_2 \Delta \psi$ for $\pi < \psi < 3\pi$ and $\frac{\Delta Z}{R} = K_2 \Delta \psi$ for $3\pi < \psi = \infty$ with Thrust Coefficient for a Two-Bladed Rotor, and a Comparison with those for a Single-Bladed Rotor
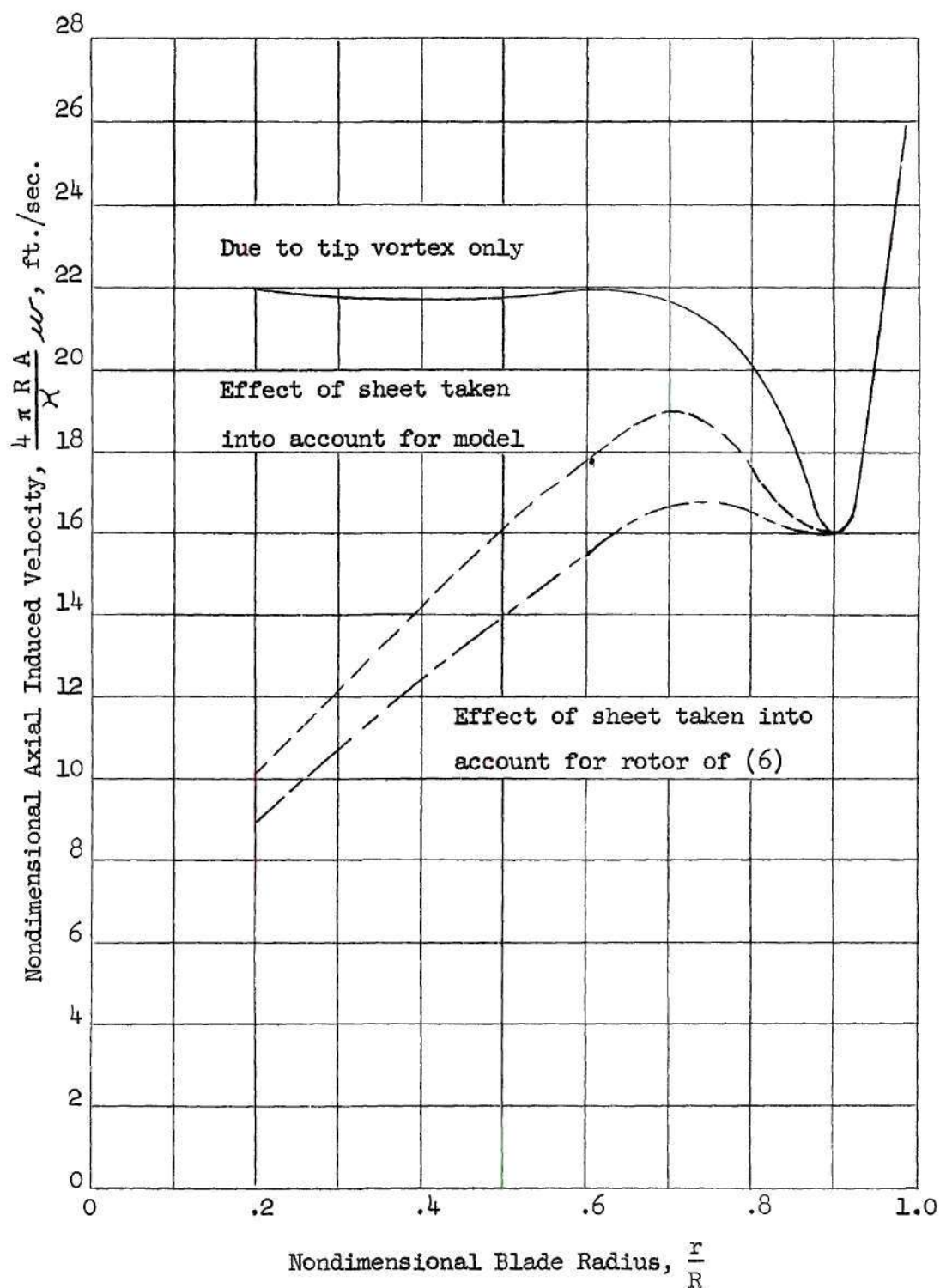
Figure 10 Theoretical Values of Nondimensional Axial Induced-Velocity

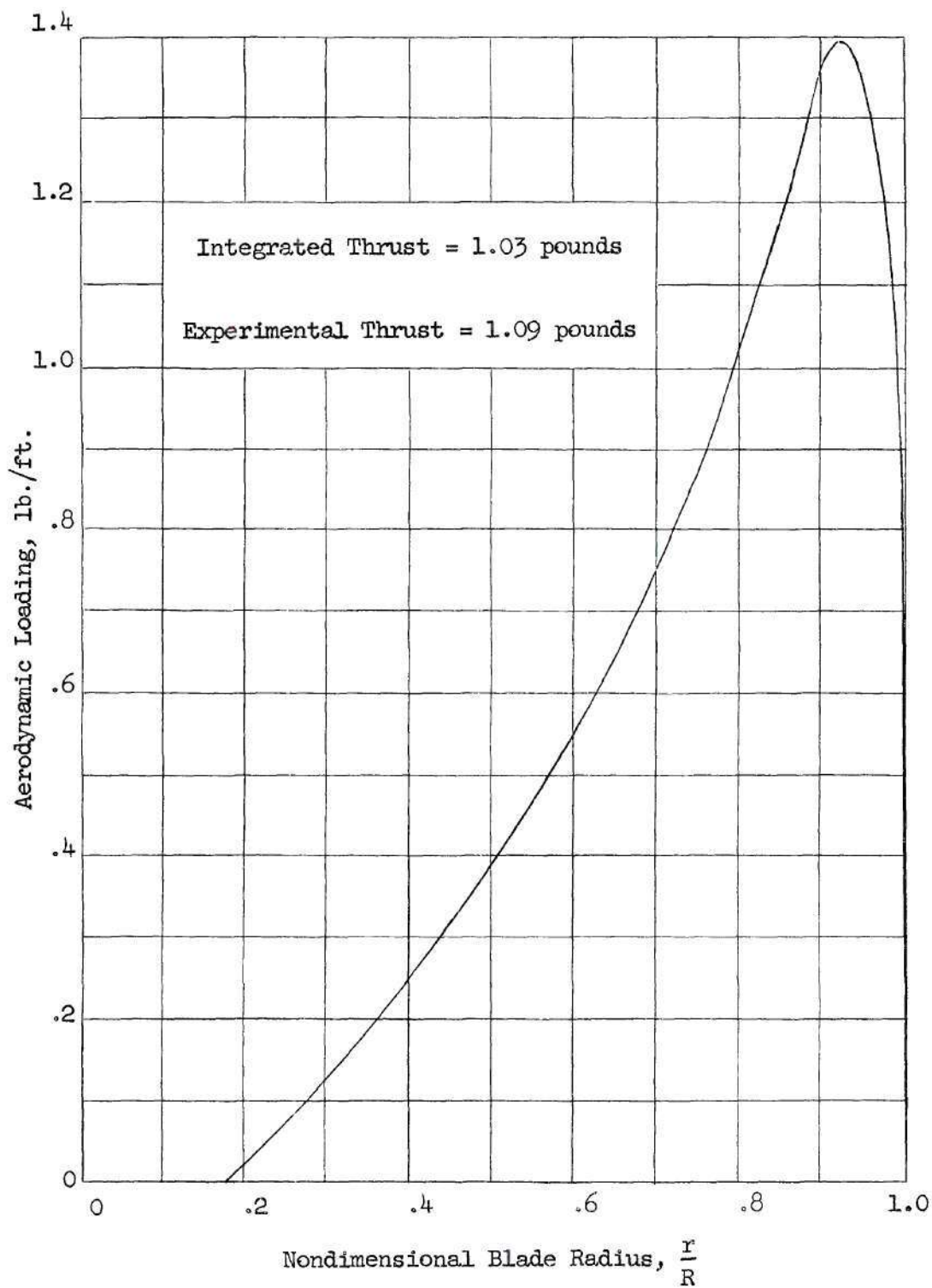Versus Nondimensional Blade Radius for a Two-Bladed Rotor

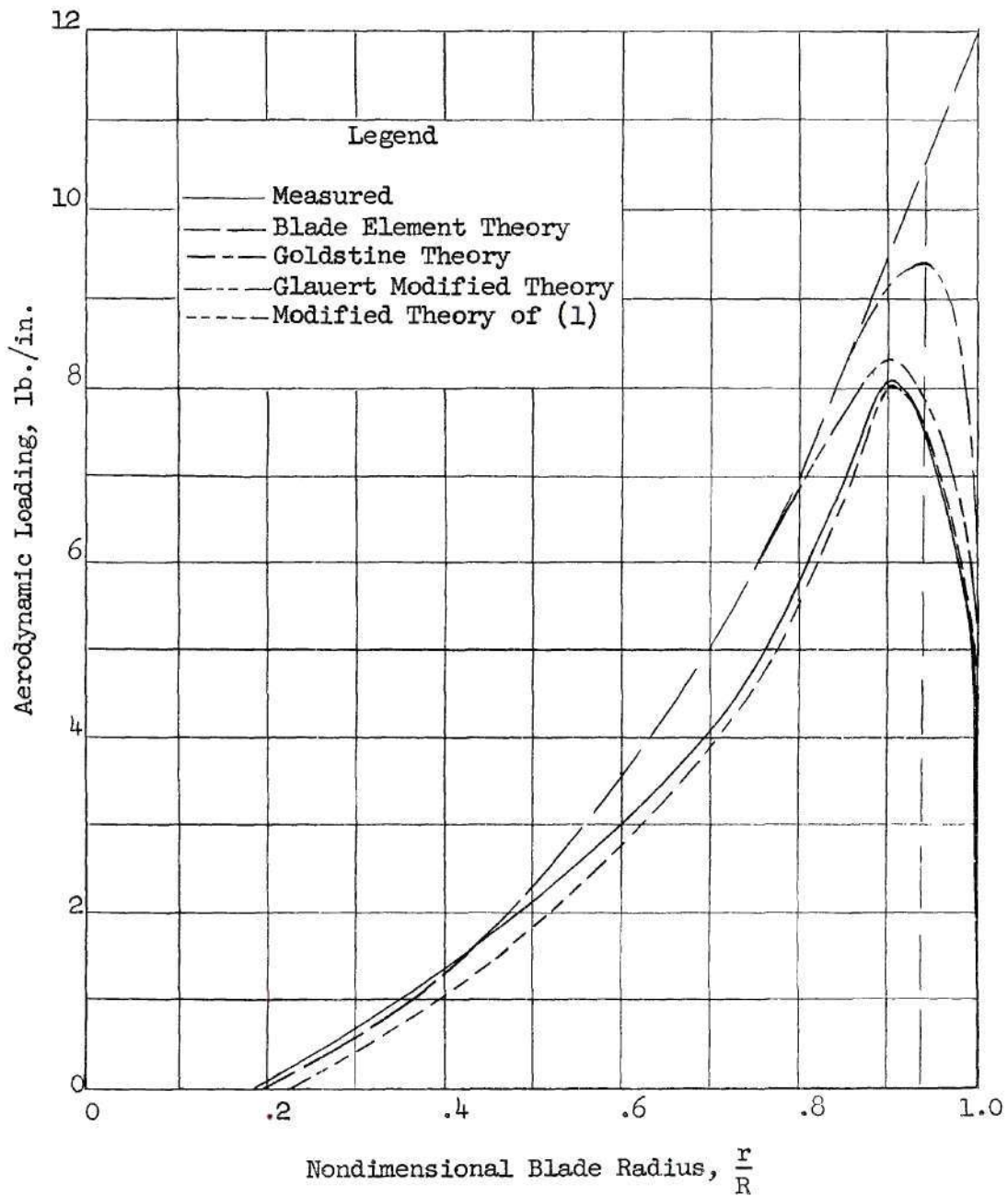Figure 11 Theoretical Model-Blade Spanwise Aerodynamic Loading

Figure 12 Comparison of Theoretical and Measured Spanwise

Aerodynamic Loadings; $\sigma = .00518$, $C_{\chi} = .0038$, $\theta = 6.68°$

BIBLIOGRAPHY

1. Gray, Robin B., *On the Motion of the Helical Vortex Shed from a Single-Bladed Hovering Model Helicopter Rotor and Its Application to the Calculation of the Spanwise Aerodynamic Loading.* Princeton University Aeronautical Engineering Department, Report No. 313, 1955.

2. Scott, James I., *An Experimental Determination of the Motion of a Vortex Sheet in the Wake of an Isolated Two-Bladed Hovering Model Helicopter Rotor.* Unpublished Masters Thesis, Georgia Institute of Technology, 1958.

3. Castles, Walter, Jr. and Gray, Robin B., *Empirical Relation between Induced Velocity, Thrust, and Rate of Descent of a Helicopter Rotor as Determined by Wind-Tunnel Tests on Four Model Rotors.* National Advisory Committee for Aeronautics, Technical Note No. 2474, 1951.

4. Jacobs, Eastman N. and Sherman, Albert, *Airfoil Section Characteristics as Affected by Variations of the Reynolds Number.* National Advisory Committee for Aeronautics, Technical Report No. 586, 1937, p. 27.

5. Heyson, Harry H. and Katzoff, S., *Normal Component of Induced Velocity in the Vicinity of a Lifting Rotor with Nonuniform Disk Loading.* National Advisory Committee for Aeronautics, Technical Note No. 3690, 1956.

6. Rabbott, John P., Jr., *Static-Thrust Measurements of the Aerodynamic Loading on a Helicopter Rotor Blade.* National Advisory Committee for Aeronautics, Technical Note No. 3688, 1956.